α decay of ^{194}At

A. N. Andreyev,[1,7,8] S. Antalic,[2] D. Ackermann,[3] L. Bianco,[4] S. Franchoo,[5] S. Heinz,[3] F. P. Heßberger,[3] S. Hofmann,[3,9] M. Huyse,[1] I. Kojouharov,[3] B. Kindler,[3] B. Lommel,[3] R. Mann,[3] K. Nishio,[6] R. D. Page,[4] J. J. Ressler,[7] P. Sapple,[4] B. Streicher,[2] Š. Šáro,[2] B. Sulignano,[3] J. Thomson,[4] P. Van Duppen,[1] and M. Venhart[2]

[1]*Instituut voor Kern- en Stralingsfysica, K.U. Leuven, University of Leuven, B-3001 Leuven, Belgium*

[2]*Department of Nuclear Physics and Biophysics, Comenius University, Bratislava, SK-84248, Slovakia*

[3]*Gesellschaft für Schwerionenforschung, Planckstrasse 1, D-64291 Darmstadt, Germany*

[4]*Department of Physics, Oliver Lodge Laboratory, University of Liverpool, Liverpool L69 7ZE, United Kingdom*

[5]*IPN Orsay, F-91406 Orsay Cedex, France*

[6]*Advanced Science Research Center, Japan Atomic Energy Agency, Tokai, Ibaraki 319-1195, Japan*

[7]*Department of Chemistry, Simon Fraser University, Burnaby, British Columbia, Canada V5A-1S6*

[8]*TRIUMF, 4004 Wesbrook Mall, Vancouver, British Columbia, Canada V6T 2A3*

[9]*Physikalisches Institut, J.W. Goethe-Universität, D-60054 Frankfurt, Germany*

(Received 4 May 2009; published 25 June 2009)

Detailed α-decay studies of the neutron-deficient isotope ^{194}At have been performed in the complete fusion reaction $^{56}\mathrm{Fe} + {}^{141}\mathrm{Pr} \rightarrow {}^{194}\mathrm{At} + 3n$ at the velocity filter SHIP. Two α-decaying isomeric states with half-lives of $T_{1/2}(^{194}\mathrm{At}^{m1}) = 310(8)$ ms and $T_{1/2}(^{194}\mathrm{At}^{m2}) = 253(10)$ ms were identified in this nucleus. Their complex decays to the states in the daughter nucleus ^{190}Bi are discussed in the article. We propose that similar to the case of the neighboring ^{191,192,193,195}At isotopes, the oblate-deformed configurations based on the proton $1/2^+[440]$ and/or $7/2^-[514]$ Nilsson orbitals become important in ^{194}At. A new isomeric state with the half-life of 175(8) ns was observed in ^{190}Bi.

DOI: 10.1103/PhysRevC.79.064320 PACS number(s): 23.60.+e, 27.70.+q, 27.80.+w

I. INTRODUCTION

Recently, a rare decay mode—the so-called Electron-Capture Delayed Fission (ECDF)—was unambiguously observed for the first time in the very neutron-deficient parent isotopes ^{192,194}At [1]. This decay mode provides unique data on low-energy fission, such as the energy and mass distribution of fission fragments, decay probabilities, and fission barrier heights for the daughter nuclei, which do not undergo spontaneous fission [2,3]. However, to be able to extract correct information on the decay probabilities, from which the fission barriers are extracted (see e.g. Ref. [4]), one needs to know spectroscopic properties such as spin and parity, along with the decay modes and branching ratios for the EC-decaying parent nucleus.

The studies of the odd-odd Tl, Bi, and At nuclei are notoriously difficult, both theoretically and experimentally, as the coupling of the odd valence neutron and odd valence proton results in multiplets of states, some members of which can become isomeric. As an example of a theoretical study of such proton-neutron (p-n) multiplets in the odd-odd Bi nuclei directly relevant to our work we refer to Ref. [5]. In many cases a relatively small energy spacing between the multiplet states strongly complicates the experimental studies, see Refs. [6–8] for examples.

In this respect α decay often offers an ideal tool to identify selectively the states in the daughter nucleus that have the same spin, parity, and configuration as in the α-decaying parent. Furthermore, in the region around the $Z = 82$ shell closure the unhindered α decay is a strong spectroscopic fingerprint for intruder states [8,9]. For example, our recent α-decay studies of the odd-odd ^{184,186,188,190}Bi [10,11] and their daughter Tl isotopes provided detailed information on the systematic appearance of the normal and intruder states in this region of the nuclidic chart. As a further extension of this work toward the odd-odd At isotopes, we recently reported on detailed α-decay studies of the very neutron-deficient new isotope ^{192}At, in which two isomeric states have been observed [12].

The present article reports on a detailed decay study of the ^{194}At nucleus. The first data on ^{194}At [$E_\alpha = 7.2 \pm 0.02$ MeV, $T_{1/2} = 180(80)$ ms] were obtained at the gas-filled separator SASSY [13]. A later study at the gas-filled separator RITU [14] suggested the existence of two isomers in ^{194}At decaying by α transitions with $E_\alpha \sim 7.14$ MeV, $T_{1/2} \sim 40$ ms and $E_\alpha \sim 7.19$ MeV, $T_{1/2} \sim 250$ ms. However, only up to 20 correlated decays were observed for this nucleus (see, Fig. 2 of Ref. [14]) and no γ decays were measured. This did not allow the authors of Ref. [14] to provide either a decay scheme or a discussion of the observed results. In our study, we collected approximately 7.5×10^4 α decays of ^{194}At, which, along with the much more advanced detection system, allowed us to deduce detailed information on this nucleus.

II. EXPERIMENTAL SETUP

The study of ^{194}At was performed using the $^{141}\mathrm{Pr}(^{56}\mathrm{Fe}, 3n)^{194}\mathrm{At}$ reaction (as in Ref. [14]). Eight 400-μg/cm^2-thick ^{141}Pr targets (100% natural enrichment) were mounted on a target wheel, rotating synchronously with the UNILAC macropulsing. The targets were produced by evaporating the $^{141}\mathrm{PrF}_3$ material onto a carbon backing of 40 μg/cm^2 thickness and covered with a 10-μg/cm^2 carbon

layer to increase the radiative cooling and reduce the sputtering of the target material. Data were taken at several beam energies, covering the energy range of the $2n$-$4n$ evaporation channels.

After separation by the velocity filter SHIP [15] the recoiling evaporation residues were implanted into a 300-μm-thick, 35×80 mm^2 16-strip position-sensitive silicon detector (PSSD), where their subsequent particle decays were measured by using standard implantation techniques [16].

The α-energy calibration of the PSSD was performed by using α lines of "by-product" nuclei, produced in the reaction through α, xn and p, xn channels and implanted in the detector: 6308(3) keV (^{191}Bi), 6699(5) keV (^{195}Po^m), 6842(6) keV (^{194}Po), and 7004(5) keV (^{193}Po^m) [17–19]. The typical α-energy resolution of each strip of the PSSD was ~23 keV (FWHM) in the energy interval of 6000–8000 keV. Because α emission is a dominant decay mode of most of the nuclei produced in this reaction, the identification of nuclides was based on the observation of genetically correlated α-decay chains, complemented by excitation function measurements.

A large-volume fourfold segmented clover germanium detector was installed behind the PSSD to measure α-γ coincidences occurring within the hardware-set time interval of $\Delta T(\alpha\text{-}\gamma) \leqslant 5$ μs. The time measurements were performed with a time-to-amplitude converter (TAC).

Three thin time-of-flight (TOF) detectors [20] were installed in front of the PSSD allowing the reaction products to be distinguished from the scattered beam particles. More importantly, decay events in the PSSD could be distinguished from the implantation events by requiring an anticoincidence condition between the signals from the PSSD and from at least one of the TOF detectors.

III. EXPERIMENTAL RESULTS

A. Identification of two isomeric states in ^{194}At

The main data for the isotope ^{194}At were collected at the beam energy of $E(^{56}\text{Fe}) = 259(1)$ MeV in front of the target, corresponding to 255 MeV in the middle of the target.

Figure 1(a) shows a part of the α-particle energy spectrum measured in the PSSD within 1500 ms after the recoil implantation. Based on half-life behavior and α-decay energies, the peaks at 6956(5) and 7004(5) keV were unambiguously assigned to ^{193}Po^{m,g} nucleus [19], produced through the $p, 3n$ evaporation channel in this reaction. The expected positions of complex α decays of ^{195}At (three α lines, [21]) and of ^{193}At (four α lines, [22]) produced in the $2n$ and $4n$ channels, respectively, are also marked in this spectrum. These isotopes were readily identified both by the α-γ coincidence analysis (see below) and by the α-α correlation analysis. For this work it is sufficient to notice that our data for ^{193,195}At are in good agreement with the results of the previous dedicated studies [21,22]. We also mention that the α-decay intensity ratio of $I(^{194}\text{At})/I(^{195}\text{At})/I(^{193}\text{At}) = 300{:}22{:}1$ was deduced at this beam energy, thus the contribution of ^{193,195}At isotopes to the spectrum of ^{194}At in Fig. 1(a) was negligible (see also the discussion and spectra below). Moreover, their contribution could be further reduced by considering α-α correlations as

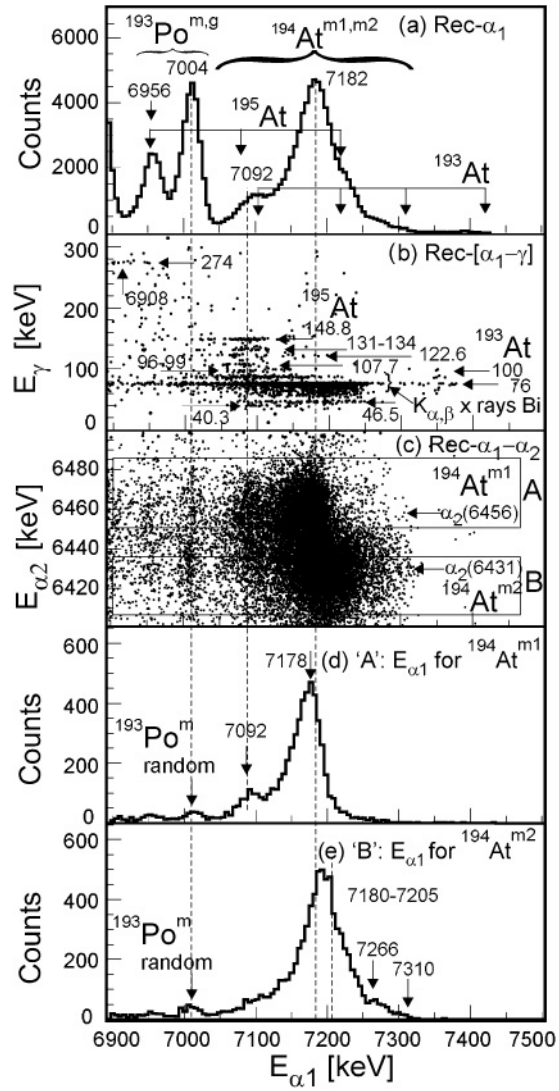

FIG. 1. (a) A part of the correlated α_1-energy spectrum for the reaction ^{56}Fe(259 MeV) + ^{141}Pr → ^{197}At* registered in the PSSD within 1500 ms after the recoil implantation. The positions of the known α-decay lines from ^{193,195}At are marked by arrows. α-decay energies are given in keV. (b) The $E_{\alpha 1}$-E_γ spectrum for α_1 events from (a) in coincidence with γ rays within the TAC time interval $0 < \Delta T(\alpha_1\text{-}\gamma) \leqslant 5$ μs. Some γ-ray groups are indicated with their energies in keV. (c) The two-dimensional $E_{\alpha 1}$-$E_{\alpha 2}$ plot for $\Delta T(\text{recoil-}\alpha_1) \leqslant 1500$ ms and $\Delta T(\alpha_1\text{-}\alpha_2) \leqslant 15$ s. Rectangles "A" and "B" denote the regions of correlations of ^{194}At with the "main"; 6456-keV α decay of ^{188}Bi^{m1} and with the main 6431-keV α decay of ^{188}Bi^{m2}, respectively. (d) The α_1-energy spectrum for the region "A" of (c). (e) The α_1-energy spectrum for the region "B" of (c).

the decay properties of their respective daughter products ^{189,191}Bi are different from that of ^{190}Bi, the daughter of ^{194}At α decay.

As shown below, the broad structure at ~7050–7310 keV, with $\sim 7.5 \times 10^4$ α decays, denoted as "^{194}At^{m1,m2}" in Fig. 1(a), is due to the complex decay of two isomeric states in ^{194}At. We note that the $E_\alpha = 7182$ keV peak within this structure is at least twice as broad as the single 7004-keV

α line of ^{193}Po^{m}, for example. This indicates that more than one line contributes to the broad 7182-keV peak.

The next step in the analysis was to search for α-γ coincidences. The $E_{\alpha 1}$-E_{γ}($\leqslant$300 keV) spectrum of α_1 events from Fig. 1(a) in coincidence with γ rays within the time interval of $\Delta T(\alpha\text{-}\gamma) \leqslant 5$ μs is given in Fig. 1(b). An additional condition was also applied that the time difference between the PSSD and the Ge clover must be nonzero [$0< \Delta T(\alpha\text{-}\gamma)$]. Though this condition effectively reduces the random background, it also suppresses the signals from the low-energy γ rays with $E_{\gamma} \leqslant 40$ keV in Fig. 1(b). This is because the timing properties of the Ge clover detectors for such low-energy γ rays are relatively poor and most of them produced no proper TAC signal in our experiment. We applied this condition in Fig. 1(b) only with the aim of demonstrating the most salient features of the α-γ spectrum under reduced background conditions. In the rest of the analysis, this condition was not applied, so the γ-ray intensity loss at low energies was avoided.

Figure 2(a) shows an expanded section of Fig. 1(b), rotated through 90°, for $E_{\gamma} \leqslant 155$ keV with a TAC condition of $\Delta T(\alpha\text{-}\gamma) \leqslant 5$ μs. The corresponding projection of Fig. 2(a) on the E_{γ} axis is given in Fig. 2(b). Due to the absence of the $0 < \Delta T(\alpha\text{-}\gamma)$ condition, several γ rays with $E_{\gamma} \leqslant 40$ keV can be seen in Fig. 2, e.g., at ~15 keV, 29.0(5) keV, and 34.9(5) keV, which are absent from Fig. 1(b).

An additional comment on Fig. 1(b) and Fig. 2 is in order here. These spectra provide the full observed α_1-γ intensity with the minimal possible conditions, thus they are used mainly for the first identification of different γ rays and α_1-γ coincidence groups and their intensity estimate. In the following, a more elaborate analysis involving stricter conditions (e.g., [α_1-γ]-α_2 correlations) will be applied. Although this will decrease the number of α_1-γ coincidence decays by at least a factor of 2 (see below), it will allow for more specific assignments to different decay branches of ^{194}At.

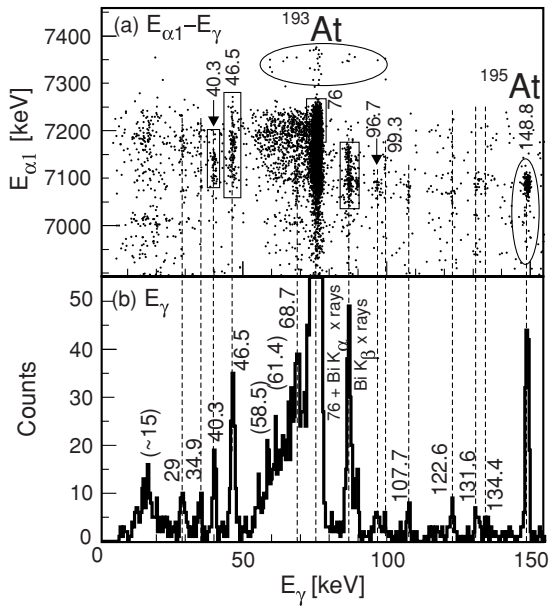

FIG. 2. (a) Expanded $E_{\alpha 1}$-E_{γ} spectrum from the recoil-[α_1-γ] analysis from Fig. 1(b) with a condition $\Delta T(\alpha_1\text{-}\gamma) \leqslant 5$ μs. γ-ray groups are indicated with their energies in keV. The decay events of ^{193,195}At are marked by the ovals. For the regions denoted by the rectangles the time distributions $\Delta T(\alpha_1\text{-}\gamma)$ are shown in Fig. 4. (b) Projection on the E_{γ} axis of the events from panel (a).

Figure 1(b) and Fig. 2 clearly show the complexity of the γ spectra, in which in addition to the Bi $K_{\alpha,\beta}$ x rays, a number of γ rays can be seen, e.g., at 29.0(5), 34.9(5), 40.3(5), 46.5(5), 68.7(5), 76.0(5), 96.7(5), 99.3(5), 107.7(5), 122.6(5), 131.6(5), 134.4(5), 148.8(5), and 274.0(5) keV [Fig. 1(b) only]. Several tentative γ rays are indicated in brackets, e.g., the γ ray at ~15 keV.

The groups of α_1(7300–7370 keV)-γ and α_1(7075 keV)-γ(148.8 keV) coincident events denoted by the ovals in Fig. 2(a) are due to ^{193}At [22] and ^{195}At [21], respectively. As no other γ rays were assigned to the decays of ^{193,195}At, either in the dedicated studies [21,22] and in the present work, all other α_1-γ coincidence groups in Fig. 1(b) and Fig. 2 must be attributed to the decay of ^{194}At.

The search for recoil-α_1-α_2 correlations is the next step in our analysis. The two-dimensional $E_{\alpha 1}$-$E_{\alpha 2}$ correlation spectrum for ΔT(recoil-α_1) $\leqslant$ 1500 ms and $\Delta T(\alpha_1\text{-}\alpha_2) \leqslant$ 15 s is shown in Fig. 1(c). It is important to realize that due to the ~50% probability of α particles escaping from the PSSD in the backward direction, the α_1-α_2 correlation analysis reduces the number of true correlated α_1 events in these spectra by approximately a factor of 2 in comparison with Fig. 1(a) (recoil-α_1 analysis). Also, if the α-decay branching ratio of the daughter nucleus is not 100%, this will further reduce the number of α_1-α_2 correlations. Despite this, the correlation with the known α_2 decays of the daughter nuclei provides a unique identification of the parent isotopes, which in most cases outweighs the disadvantage of the intensity reduction.

In our analysis, the identification of different decays of ^{194}At was performed by using their time-position correlations with the strongest known α decays of two isomeric states in the daughter nucleus ^{190}Bi with the tentative spin and parity assignments of (10^{-}) and (3^{+}) [7,8,10]. A recent mass-measurement with the ISOLTRAP setup at ISOLDE-CERN [23] attempted to deduce the relative position of these isomers and to establish which one of them is the ground state. However, as the authors of work [23] reported: "Due to the minor resolution during the measurement, a mixture of both states ^{190}Bi and ^{190}Bi^{m} differing by $E = 150(190)$ keV might be present." In other words, the quoted precision does not allow the relative positions of the isomers in ^{190}Bi to be established unambiguously.

In the present work we therefore use the same denotations for the isomers in ^{190}Bi as used in our recent study [10]. Namely the higher-spin (10^{-}) isomer ($E_{\alpha} = 6456(5)$ keV, $T_{1/2} = 6.2(1)$ s, $b_{\alpha} = 70(9)\%$ [7,8]) will be referred to as ^{190m1}Bi, while the low-spin (3^{+}) isomer ($E_{\alpha} = 6431(5)$ keV, $T_{1/2} = 6.3(1)$ s, $b_{\alpha} = (90^{+10}_{-30})\%$ [7,8]) will be denoted as ^{190m2}Bi. Thus, the α_1 events in the region denoted by a rectangle "A" of Fig. 1(c) correlate with the strongest ($I_{\rm rel} = 98\%$) $E_{\alpha} = 6456$ keV decay of ^{190}Bi^{m1}, while the α_1 events in the rectangle "B" correlate with the strongest ($I_{\rm rel} = 96\%$) $E_{\alpha} = 6431$ keV decay of ^{190}Bi^{m2} (see also Fig. 7).

Note that for the following analysis we explicitly exclude the region of $E_{\alpha 2} = 6436$–6450 keV between the rectangles "A" and "B." In this way we are able to separate more reliably the correlations of the ^{194}At decays with the α decays of different isomers in the daughter nucleus ^{190}Bi.

Figures 1(d) and 1(e) show the $E_{\alpha 1}$ energy spectra for the events from the rectangles "A" ($E_{\alpha 2} = 6456$ keV) and "B" ($E_{\alpha 2} = 6431$ keV) of Fig. 1(c), respectively. First, we notice the presence of small peaks at $E_{\alpha 1} = 7004$ keV in these spectra, which are marked as "^{193}Po^{m}, random." These peaks are due to the random recoil-α_1(7004 keV)-α_2 correlations of the 7004-keV decay of ^{193}Po^{m} with either 6456 keV [Fig. 1(d)] or 6431 keV [Fig. 1(e)] α decays of ^{190}Bi^{m1,m2}. Such events are indeed random, as the daughter product of ^{193}Po^{m}—the ^{189}Pb nucleus—has no α decays in the energy interval of 6431–6456 keV. Both the long correlation time interval of $\Delta T(\alpha_1$-$\alpha_2) \leqslant 15$ s and a relatively high counting rate of α decays in the PSSD lead to random correlations, whose number can be reliably estimated by comparing the intensity of the true rec-α_1(7004 keV) correlations from Fig. 1(a) with the number of random rec-α_1(7004 keV)-α_2(6431 or 6456 keV) correlations from Figs. 1(d) and 1(e). Based on this comparison, we estimate that the random correlations may contribute at most at a level of 0.6(1)% to α decays of ^{194}At in the energy interval of 7050–7400 in Figs. 1(c)–1(e).

The different spectra shapes at $E_{\alpha 1} \geqslant 7050$ keV in Fig. 1(d) and Fig. 1(e) hint that two α-decaying isomeric states exist in the parent nucleus ^{194}At, in such a way that one of them decays predominantly to ^{190}Bi^{m1}, while the other decays predominantly to ^{190}Bi^{m2}.

The presence of two isomeric states in ^{194}At is further corroborated by the different half-life values deduced for the α_1 events from the rectangles "A" and "B," respectively. Figure 3 shows the time distributions ΔT(recoil-[α_1-α_2]) between the recoil implantation and a pair of subsequent correlated α_1-α_2 decays for the events from the regions

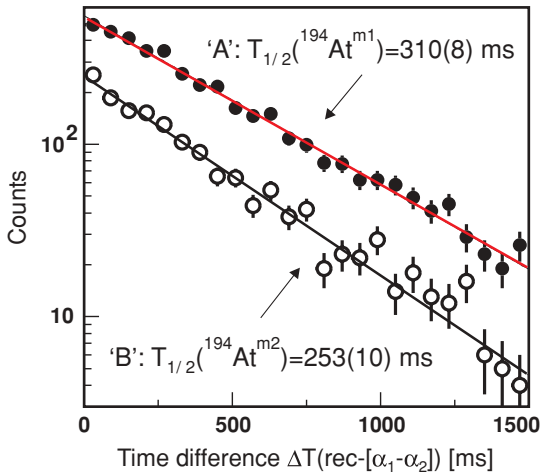

FIG. 3. (Color online) Time difference ΔT(recoil-[α_1-α_2]) for events from the regions "1A" and "1B" of Fig. 1(c) with the condition of $E_{\alpha 2} \geqslant 7050$ keV. The α_2(6431 keV)-γ(294 keV) coincident events have been used to produce the decay curve for ^{194}At^{m2}; see text for details. The data and the exponential fits are shown by the symbols and solid lines, respectively.

"A" and "B" of Fig. 1(c) with a condition of $E_{\alpha 2} \geqslant 7050$ keV. To avoid a possible contribution of the low-energy tail of the 6456 keV α decay of ^{190}Bi^{m1} in the spectrum produced for the 6431-keV decay of ^{190}Bi^{m2}, an extra condition was applied exploiting the fact that the 6431-keV decay has strong coincidences with the 294-keV $E1$ transition in ^{186}Tl [10] (see, also Fig. 7, right panel). Therefore, the recoil-α_1-[α_2(6431 keV)-γ(294 keV)] analysis was used to deduce the half-life of ^{194}At^{m2}. The time distributions in Fig. 3 can be fitted with a single exponential function with the half-life values of $T_{1/2} = 310(8)$ ms (region "A") and $T_{1/2} = 253(10)$ ms (region "B"). This analysis was also repeated by applying a "running" α_2 energy window with a width of 20 keV, which showed the stability of the deduced half-half value.

Thus, two different half-life values for decays attributed to ^{194}At identify two α-decaying isomeric states in this nucleus. The 310(8) ms isomer decaying to ^{190}Bi^{m1} will further be denoted as ^{194}At^{m1} (events in "A"), while the 253(10) ms isomer decaying to ^{190}Bi^{m2} will be denoted as ^{194}At^{m2} [events in "B" of Fig. 1(c)].

No evidence for the $T_{1/2} \sim 40$ ms, $E_{\alpha} \sim 7.14$ MeV α-decaying isomer proposed in Ref. [14] for ^{194}At could be seen in our data despite more than three orders of magnitude higher number of decays. Therefore, we rule out the presence of the ~40 ms isomeric state in ^{194}At. A possible contribution of ^{193}At, which has three isomeric states with the half-lives of 20–30 ms and α-decay energies comparable to ^{194}At [see Fig. 1(a)] could be a source of ~40 ms events observed in Ref. [14].

B. Isomeric 76-keV γ ray in ^{190}Bi

Figures 1(b) and 2 show an interesting feature, which is important for the following discussion: the strong 76.0(5) keV γ ray that is in coincidence with a broad α_1 group with an apparent energy of $6900 \leqslant E_{\alpha 1} \leqslant 7255$ keV. We clearly distinguish this γ-ray transition from the Bi K_{α} x rays at 77.1 keV (46.2%, $K_{\alpha 1}$) and 74.8 keV (27.7%, $K_{\alpha 2}$) [17]. The main argument for this inference, apart from the energy difference, comes from an unexpectedly high intensity ratio of K_{α} and K_{β} x rays $I(K_{\alpha})/I(K_{\beta}) \sim 22(2)$ that would be obtained if one assumed that the peak at 76 keV was due to the Bi K_{α} x rays only. This ratio is much higher than the literature ratio of $I(K_{\alpha})/I(K_{\beta}) \sim 3.7$ [17].

Figure 4 gives the time distribution between the α_1 decay and coincident γ ray for several groups of events from Fig. 2(a) marked by rectangles: 40.3, 46.5, and Bi K_{β} x rays. As a reference, Fig. 4(a) also shows the symmetric "bell-like" time behavior of the known $E_{\gamma} = 294$ keV $E1$ decay of ^{186}Tl with the reported half-life value of $T_{1/2} = 11$ ns [8], which is in coincidence with the 6431-keV decay of ^{190}Bi^{m2} (not shown in the spectra in this work). Within the timing resolution of our electronics system and Ge clover detectors, we consider this γ-ray transition to be "prompt." Figure 4(b) gives the time behavior of the 76-keV γ rays measured in coincidence with the α particles in the limited region of $E_{\alpha} = 7170$–7255 keV. This energy interval was specifically chosen to avoid the contribution from the lower-energy α decays of ^{194}At which occur in coincidence with prompt partially K-converted γ rays

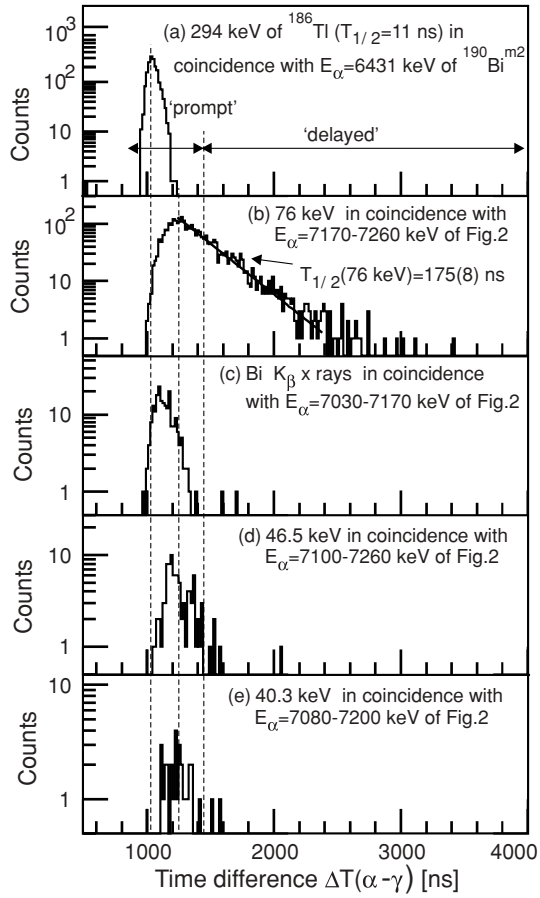

FIG. 4. The time difference $\Delta T(\alpha\text{-}\gamma)$ between the coincident α and γ decays from recoil-[α_1-γ] analysis (see text for details). (a) α(6431 keV)-γ(294 keV) decay of ^{190}Bi^{m2}. The definitions of the "prompt" and "delayed" time windows are shown (see text for details); (b) 76-keV $E1$ decay in ^{190}Bi, an exponential fit is shown by the solid line. (c) K_β Bi x rays; (d) 46.5-keV $M1$ decay in ^{190}Bi; (e) 40.3-keV decay in ^{190}Bi.

of ^{190}Bi, as discussed below. For example, the time distribution for the respective Bi K_β x rays in Fig. 4(c) indeed shows no evidence for any delay and is similar to that of the "prompt" 294-keV γ decay in Fig. 4(a).

The decay curve of the 76-keV decay was fitted with a single exponential resulting in a half-life value of 175(8) ns. This identifies a new isomeric state in ^{190}Bi, which will be discussed further below.

In the following discussion we will often use two different α-γ time coincidence intervals, defined in Fig. 4(a), which will allow us to clearly distinguish prompt and delayed γ rays. Namely the events which occur within the time window of $\Delta T(\alpha\text{-}\gamma) \leqslant 1450$ ns will be considered as "prompt," while the events in the time interval of 1450 ns $\leqslant \Delta T(\alpha\text{-}\gamma) \leqslant 5000$ ns will be considered as "delayed." Note that the prompt peak for the 294-keV γ ray in Fig. 4(a) starts at a value of ∼980 ns, defined by the delay circuit in our electronics.

C. ^{194}At^{m2} → ^{190}Bi^{m2} decay (right panel of Fig. 7)

The decay scheme of ^{194}At^{m2} was built based on the recoil-α_1-α_2($\leqslant$6436 keV) and recoil-[α_1-γ]-α_2($\leqslant$6436 keV) correlation analysis, see Figs. 5(a)–5(f). For convenience of the discussion, Fig. 5(a) reproduces the α_1-spectrum from Fig. 1(e) [α_1 events from the rectangle "B" of Fig. 1(c)]. The broad "flat-top" peak at ∼7180–7205 keV with the higher-energy tail extending up to ∼7310 keV can be seen in the spectrum. Those events from Fig. 5(a) that are in prompt coincidence with γ decays with $E_\gamma \leqslant 150$ keV are shown in the two-dimensional $E_{\alpha 1}$-E_γ plot in Fig. 5(b), while the corresponding projection on the E_γ axis is given in Fig. 6(a). As one can see, apart from the weak $K_{\alpha,\beta}$ Bi x rays, the main coincident γ rays for the α decays of ^{194}At^{m2} are at 76 and 46.5 keV and, possibly, at ∼15, 29, and 132 keV. There could also be weaker groups of γ rays at ∼60–65 keV, but due to low intensity we cannot unambiguously assign them to the decay of ^{194}At. However, all these γ rays are present in Figs. 1(b) and 2, which show the result of the recoil-[α_1-γ] analysis only where they have higher statistics. Thus, we conclude that most probably even the weakest γ lines in Figs. 5(b) and 6(a) represent γ decays following the fine-structure α decays of ^{194}At^{m2}.

Figures 5(c) and 5(d) show the projections on the $E_{\alpha 1}$ axis for the α_1 decays in prompt coincidence with the 76- and 46.5-keV γ decays of Fig. 5(b). These regions are marked by the rectangles in Fig. 5(b). As seen in Figs. 5(b) and 5(c), the 76-keV γ decay is in coincidence with the broad region of α_1 decays in the interval of ∼6900–7250 keV. By comparing the number of recoil-α_1(7050–7250 keV) events from Fig. 5(a) and the number of recoil-[α(7050–7250)-γ(76 keV)] events from Fig. 5(b), corrected for the γ detection efficiency at 76 keV, a total conversion coefficient of $\alpha_{\rm tot}(76\ {\rm keV}) = 0.4(1)$ was deduced. This unambiguously establishes an $E1$ multipolarity for the 76-keV γ ray as the theoretical conversion coefficient is $\alpha_{\rm tot}(E1) = 0.2$ [24]. An $M1$ multipolarity [$\alpha_{\rm tot}(M1) = 4.24$] and all higher multipolarities must be ruled out due to their much higher conversion coefficients, which would be incompatible with the observed numbers of α and α-γ(76 keV) decays in the spectra.

More generally, the intensity ratio between Fig. 5(a) (α_1-α_2) and Fig. 5(c) ([α_1-γ]-α_2) is ∼13(2), which is readily explained by the above partial conversion of the 76-keV transition and by the Ge detector efficiency at this γ-ray energy. On these grounds a very important conclusion has been drawn that most of the α decays of ^{194}At^{m2} in Fig. 5(a) are followed by the 76-keV γ decay, the fact that is crucial for the construction of the decay scheme; see Fig. 7.

The α-γ spectrum of delayed coincidences [1450 ns $\leqslant \Delta T(\alpha\text{-}\gamma) \leqslant 5000$ ns] for ^{194}At^{m2} is shown in Fig. 5(e). It clearly demonstrates an important fact, mentioned above, that apart from 76-keV decay, there are no other delayed γ rays or Bi K x rays present. The corresponding energy distribution of α decays in delayed coincidences with the 76 keV γ rays is shown in Fig. 5(f), in which the peaks at 7195(15) keV and 7230(15) keV and a weak peak at 7145 keV are seen.

Before we proceed with further discussion of spectra and of the proposed decay scheme for ^{194}At^{m2}, a comment must be made on the important effect of the α-e^- energy summing in a silicon detector of the coincident α decay and subsequent conversion electrons in case the α decay populates an excited state. To our knowledge, this effect was first mentioned in

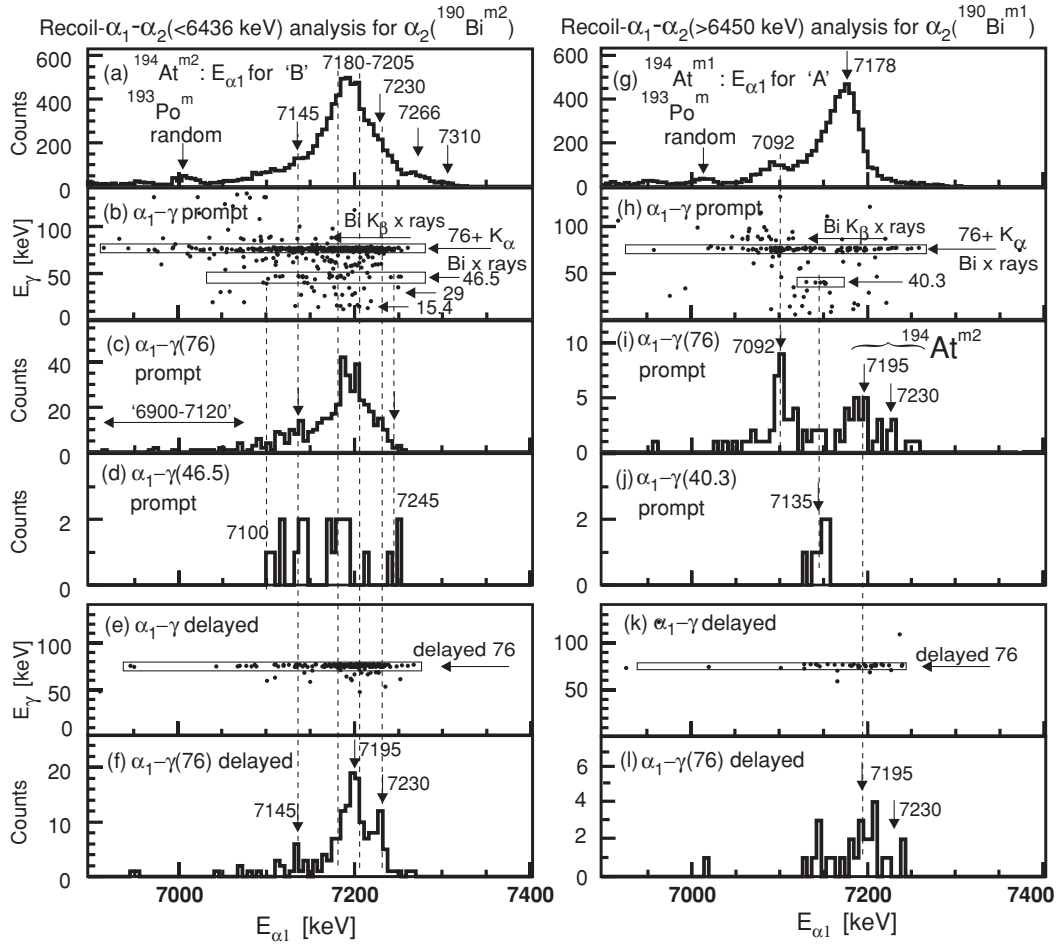

FIG. 5. Recoil-α_1-α_2 and recoil-[α_1-γ]-α_2 analysis for ^{194}At^{m2} (left column) and ^{194}At^{m1} (right column). [(a) and (g)] α_1 spectra from recoil-α_1-α_2 analysis [the copies of Figs. 1(e) and (d), respectively]. [(b) and (h)] 2D α_1-γ spectra within the prompt coincidence time $\Delta T(\alpha_1\text{-}\gamma) \leqslant$ 1450 ns. For the regions denoted by rectangles the projections on the $E_{\alpha 1}$ axis are shown in the following panels. [(c) and (i)] Projections on the $E_{\alpha 1}$ axis of events in prompt coincidence with the 76-keV γ rays. [(d) and (j)] Projections on the $E_{\alpha 1}$ axis of events in prompt coincidence with the 46.5- and 40.3-keV γ rays, respectively. Panels (e)/(f) and (k)/(l) show the delayed spectra for ^{194}At^{m1,m2} within the time interval of 1450 ns $\leqslant \Delta T(\alpha_1\text{-}\gamma) \leqslant$ 5000 ns. See the main text for details.

Ref. [25] and recently discussed in more detail in our studies of the odd-odd isotopes ^{184,186,188,190}Bi [10,11] and ^{192}At [12] for which such an effect is notoriously conspicuous.

Such energy summing in the PSSD is a well-known effect in experiments at recoil separators, when the recoil is implanted in the PSSD at a typical implantation depth of a few micrometers. If both the α particle and the conversion electron stop in the PSSD, then the full α-e^- energy summing happens resulting in an "artificial" α peak, which is often mistaken as a real α decay of a nucleus, see detailed discussion in Ref. [25]. If the electron escapes from the PSSD in the backward direction, an emission-angle-dependent *partial* α-e^- energy summing in the PSSD happens, which produces the broadly distributed energy peak between the original α peak and the full energy summing peak mentioned above. Actually, the *lowest possible* energy summing happens in case when the electron escapes normally to the PSSD surface with a typical energy deposition of ~5–10 keV [26] in the PSSD in the case of a typical recoil implantation depth of a few micrometers and electron energies of up to a few hundreds of keV. For simplicity of the following discussion we adopt a value of 5 keV for this "minimal" summing, which must be taken into account when deducing the "proper" unperturbed α-decay energy in the case of α-electron summing.

With the above considerations, we interpret the peaks at 7195 and 7230 keV in Fig. 5(f) as follows. First, we assume that there is a 7190(15)-keV α decay of ^{194}At^{m2}, which is in delayed coincidence with the 76-keV γ rays. The energy difference of 5 keV between the observed peak at 7195 keV and the adopted ("corrected") energy of 7190 keV is due to the α-e^- summing with the conversion electrons from the strongly converted "45(15) keV" decay. The latter γ transition must be introduced to account for the features seen in Fig. 5(a) and, in particular, in Fig. 5(f). First of all, this "extra" transition is necessary to account for the difference of ~45(15) keV between the sum energy of α(7190 keV) + γ(76 keV) ~ 7266 keV and the maximum energy α decays at 7310 keV in Fig. 5(a). The ~45(15) keV γ decay was not observed in our

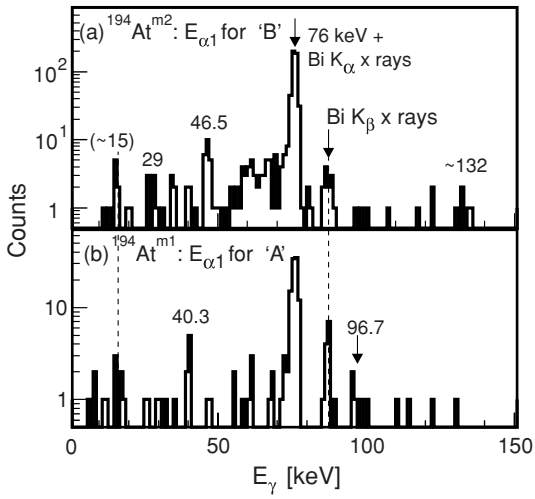

FIG. 6. (a) Projection on the E_γ axis of all prompt coincident events from Fig. 5(b). (b) The same for events from Fig. 5(h). Some γ-ray groups are indicated with their energies in keV.

spectra (the 46.5-keV decay is different and will be discussed below), presumably due to its strong internal conversion, which would result in the L- and M-conversion electrons with the energies of ∼30 and ∼42 keV, respectively (the L/M ratio is ∼4). Then, the α(7190 keV) $+e^-(L, M)$ summing in the PSSD with these electrons will naturally produce the apparent peak at 7230 keV in Fig. 5(f) and also as a higher-energy shoulder above the peak at 7180–7205 keV in Figs. 5(a) and 5(c).

Based on these arguments, the decay sequence following the 7190-keV α decay of ^{194}At^{m2} was constructed; see Fig. 7. Note that the weak peak at 7266 keV in Fig. 5(a) is readily explained as due to the 7266-keV α decay feeding to the "45(15) keV" state in ^{190}Bi^{m2}. The intensity balance for the unobserved "45(15) keV" γ-ray transition strongly suggests that it must be of $M1$ multipolarity, as any higher multipolarity has too high a conversion coefficient, which would result in the α-decay intensity of the coincident α decays being much higher than the *total* intensity in Fig. 5(a).

Now, we return to Fig. 5(d), which shows the α decays in prompt coincidence with the 46.5-keV transition. We assume that this γ ray is in coincidence with the weak 7145(15)-keV α decay, seen in Figs. 5(a) and 5(b). Indeed, the total Q_α (7145 keV) $+E_\gamma$(46.5 keV) value for this coincident pair matches well the Q_α value for the "main" 7190-keV α decay. Based on these arguments, the α(7145 keV) + γ (46.5 keV) coincident decay was placed in the decay scheme of ^{194}At^{m2} as shown in Fig. 7. We also observed coincidences between the 76- and 46.5-keV γ decays, which strengthens the above inference. Similarly to the 76-keV decay, the intensity balance (which includes the corrections both due to the possible internal conversion and due to the γ-ray detection efficiency) strongly suggests an $E1$ multipolarity for the 46.5-keV decay.

Altogether, the three γ transitions at 76, 46.5, and "45(15) keV" and their conversion electrons account well for the observed features of the spectra in Figs. 5(a)–5(f). For example, the broad α-decay energy distribution in Fig. 5(d) [in coincidence with γ(46.5 keV)] can be naturally explained by summing with the conversion electrons from the 76-keV and "45(15)"-keV decays.

Several low-intensity fine-structure α decays should exist in ^{194}At^{m2} with energies in the range of ∼6900–7120 keV. This is based on observed coincidences of the ∼6900–7120 keV decays with the 76-keV γ transition, see Figs. 5(b) and 5(c). Furthermore, in Fig. 2 several such α decays are clearly seen in coincidence with a number of γ rays with $E_\gamma = 90$–140 keV. Some of these transitions must be K-converted [the K-shell electron binding energy in Bi is $B_e(K) = 90.5$ keV] as weak Bi K_β x rays are seen in Figs. 2, 5(b), and 6(a). The prompt character of these Bi K_β x rays [see Fig. 4(c)] suggests that the corresponding γ-ray transitions do not originate from the 175 ns isomeric state in ^{190}Bi. Unfortunately, due to low statistics a γ-γ coincidence analysis was not possible and we are unable to provide an unambiguous placement of these γ-ray transitions. The corresponding feeding α decays are collectively denoted as "6900–7120 keV" in Fig. 5(c), but they are not shown in the decay scheme of ^{194}At^{m2} in Fig. 7. The deduced decay data for ^{194}At^{m2} are summarized in Table I and will be discussed further below.

D. ^{194}At^{m1} → ^{190}Bi^{m1} decay (left panel of Fig. 7)

A very similar analysis was performed for the $T_{1/2} = 310(8)$ ms ^{194}At^{m1} isomer [events in "A" of Fig. 1(c)]. The decay scheme for this isomer was built based on the recoil-α_1-α_2(⩾6450 keV) and recoil-[α_1-γ]-α_2(⩾6450 keV) correlation analysis by specifically searching for its correlated decays with the 6456-keV α decay of the daughter ^{190}Bi^{m1} isomeric state; see Fig. 7. The corresponding spectra, shown in Figs. 5(g)–5(l) and Fig. 6(b), were produced with the same timing conditions as the spectra for ^{194}At^{m2} in Figs. 5(a)–5(f) and Fig. 6(a). Therefore, only a brief discussion of the most salient and relevant features of ^{194}At^{m1} will be given here.

Figure 5(g) shows that the two strongest decay of ^{194}At^{m1} have energies of 7178(15) and 7092(15) keV. However, we notice that a group of prompt α(7085 keV)-γ (96.7 keV) coincident events is present in Fig. 2(a). The total Q_α(7085 keV) + E_γ(96.7 keV) value matches well the Q_α value for the 7178-keV α decay of ^{194}At^{m1}, which is why it was placed in the decay scheme of ^{194}At^{m1} as shown in Fig. 7. Based on these arguments, we interpret the observed 7092-keV decay in Figs. 5(g)–5(i) as arising from the α(7085 keV) + e^-(6.5 keV) summing in the PSSD. The 6.5-keV conversion electrons are produced as a result of the strong K-shell internal conversion of the 96.7-keV γ transition (e.g., $\alpha_K(M1) = 9$ [24]). The strong conversion is confirmed by the observation of the summed 7092-keV decay in prompt coincidences with the Bi K_α x rays, see Figs. 5(h) and 5(i). Due to their low energies, the conversion electrons are fully registered in the PSSD, which results in the shifted full energy summing peak of ∼7092 keV, as seen in our data. The intensity balance for α and α-γ(96.7 keV) events established an $M1$ multipolarity for the 96.7-keV decay.

Similarly, Figs. 5(h) and 5(j) show the group of prompt α(7135 keV) + γ(40.3 keV) coincident events. The total

TABLE I. The measured decay properties of ^{194}At. Shown are isomer assignments, α-decay energies E_α, relative intensities I_α, reduced α-decay widths δ^2_α, and hindrance factors HF_α, energies and multipolarities of coincident γ rays. The typical γ-ray energy uncertainty is 0.5 keV. The reduced α-decay widths were calculated with the Rasmussen prescription [30] by assuming $\Delta L = 0$ decays. The hindrance factors are shown relative to the strongest 7178- and 7190-keV decays of each isomer, for which $HF_\alpha = 1$ was assumed (see also discussion in the text). All multipolarity assignments are tentative and are based on the measured internal conversion coefficients.

Isomer, $T_{1/2}$ (ms)	E_α (keV)	I_α (%)	δ^2_α (keV)	HF_α	Coincident γ rays[a] (keV)
^{194}At^{m1},	6908(15)	1.0(3)	1.1(4)	9(3)	274(1) $E2$
310(8) ms	7087(15)	13(2)	3.5(7)	2.9(6)	96.7 $M1$, Bi K x rays
	7135(15)	8(2)	1.5(4)	6.7(20)	40.3 $E1$
	7178(15)	78(5)	10.0(14)	1	
^{194}At^{m2},	7145(15)	9(3)	2.0(7)	6(2)	Bi K x rays, 46.5 $E1$, 76 $E1$
253(10) ms	7190(15)	83(3)	12(1)	1	76 $E1$, "45(15)"[b] $M1$
	7266(15)	7(3)	0.6(3)	20(10)	"45(15)"[b] $M1$
	7310(15)	$\leqslant$1.0(5)	$\leqslant$0.06(2)	$\geqslant$200(100)	

[a]As discussed in Sec. III A, the following γ rays should also follow the α decay of ^{194}At: ~15, 34.9(5), 68.7(5), 99.3(5), 107.7(5), 122.6(5), 131.6(5), and 134.4(5) keV.
[b]Unobserved, presumably strongly converted transition; see text for details.

$Q_\alpha(7135\text{ keV}) + E_\gamma(40.3\text{ keV})$ value matches well the Q_α value for the 7178-keV α decay of ^{194}At^{m1}. Therefore this coincident decay was also assigned to ^{194}At^{m1} as shown in Fig. 7. An $E1$ multipolariy was deduced for the 40.3-keV decay based on intensity balance arguments.

Finally, the α(6908 keV)-γ(274(1) keV) group with ~15 decays is seen in Fig. 1(b), which is further correlated with the 6456-keV decay of ^{190}Bi^{m1}, but not with the 6431-keV decay of ^{190}Bi^{m2}. Thus, the 274(1)-keV γ ray must be placed on top of the (10^-) isomer ^{190}Bi^{m1}. The total Q_α value for the α(6908 keV)-γ(274 keV) decay $Q_{\text{total}} = 7327(15)$ keV matches well the value of $Q_\alpha = 7326(15)$ keV for the strongest 7178(15) keV α decay of ^{194}At^{m1}. On these grounds the α(6908 keV)-γ(274 keV) decay was placed in parallel with the 7178-keV decay, as shown in Fig. 7. We assume that this 274(1)-keV γ transition is the same as the 273(1)-keV isomeric γ decay identified in our earlier study and placed directly on top of the (10^-) isomer of ^{190}Bi; see Ref. [27]. Based on the limited statistics available in the present study a half-life value of $T_{1/2}(274\text{ keV}) = 1^{+1}_{-0.5}$ μs was derived, which is consistent with the lower limit of $T_{1/2}(274\text{ keV}) \geqslant 500(100)$ ns estimated in Ref. [27]. The deduced half-life value limits the possible multipolarity for the 274-keV decay as $E1$, $M1$, $E2$, or $M2$.

The K-conversion coefficient of $\alpha_K = 0.20(5)$ was also estimated for this decay in Ref. [27]. This excludes an $M2$ multipolarity as the calculated K-conversion coefficient is too high ($\alpha_{\text{calc.}}(M2) = 1.72$ [24]). An $E1$ multipolarity should also be excluded as both its calculated conversion coefficient is too low [$\alpha_{\text{calc.}}(E1) = 0.03$] and its half-life is expected to be much shorter than observed.

However, the measured conversion coefficient is between the theoretical K-conversion coefficients of $\alpha_{\text{calc.}}(E2) = 0.08$ and $\alpha_{\text{calc.}}(M1) = 0.49$. A pure $M1$ multipolarity should be excluded as an 274-keV $M1$ transition is not expected to be isomeric. Based both on the Weisskopf single-particle half-life calculations [17] and the experimental K-conversion coefficient, the most plausible multipolatiry for the 274-keV decay should be an $E2$ or, possibly, a mixed $M1 + E2$ multipolarity.

Last, but not least, we want to discuss the groups of prompt and delayed α(7195–7230 keV)-γ(76 keV) coincident events in Figs. 5(h), 5(i), 5(k), and 5(l). One can easily see that both the energy and the spectrum shape of this group matches well those of a similar group of events in Figs. 5(c), 5(e), and 5(f) (decay of ^{194}At^{m2}). The only marked difference is in the intensity of these groups in the spectra on the left and on the right sides of Fig. 5, with the ratio of intensities being ~10 times in favor of ^{194}At^{m2}.

We interpret the α(7195–7230 keV)-γ(76 keV) in Figs. 5(h)–5(l) as due to random correlations of α_1 decays of ^{194}At^{m2} with the α_2 decays in the region of 6450–6580 keV, which coincides with the region of α decays of ^{190}Bi^{m1}. This is because the strongest 6431-keV decay of ^{190}Bi^{m2} is in coincidence with 294- and 79-keV γ decays [8], as schematically shown in Fig. 7. The internal conversion of both transitions will produce the conversion electrons, which will sum up in the PSSD with the energy of the feeding 6431-keV decay. This produces the higher-energy tail of the 6431-keV decay of ^{190}Bi^{m2}, which will partially "overlap" with the 6456-keV decay of ^{190}Bi^{m1}, used to produce correlation spectra of ^{194}At^{m1} (right panel of Fig. 5). Unfortunately, the branching ratio between the 294-keV $E1$ decay and the 79-keV decay of unknown multipolarity is not known experimentally. This prevents us from making a quantitative analysis of the summing probability and the sum energy spectrum. However, we mention here that the total conversion coefficient for the 294-keV $E1$ transitions is $\alpha_{\text{tot}}(E1) = 0.03$ [24], thus the summing effect due to this transition alone could be quite large. The total conversion coefficient for the 79-keV decay is $\alpha_{\text{tot}} = 0.18$ if one assumes an $E1$ multipolarity. Any higher multipolarity has much higher total conversion coefficient [e.g., $\alpha_{\text{tot}}(M1) = 3.93$], which would lead to even larger

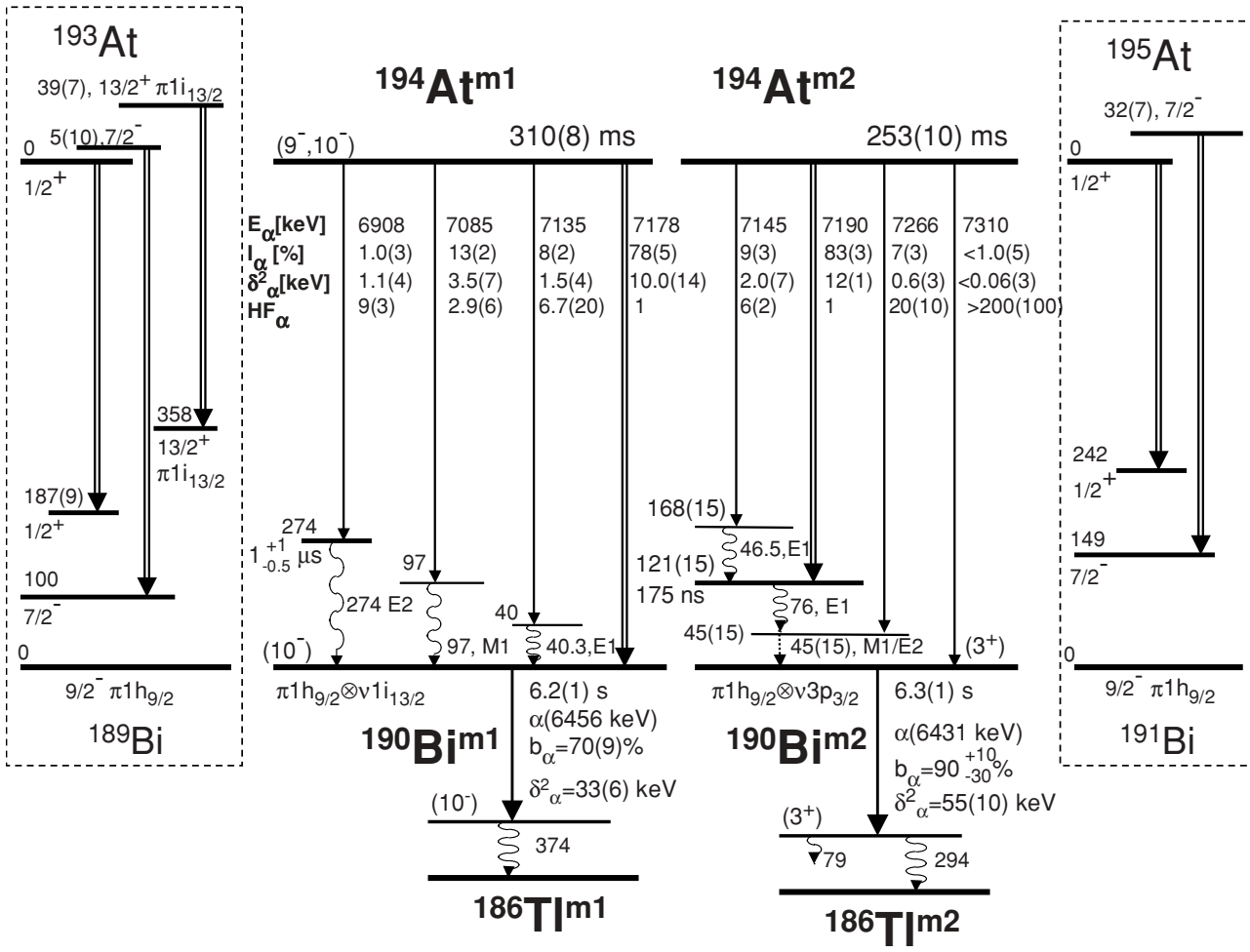

FIG. 7. Decay schemes of the ^{194}At^{m1,m2} isomers deduced in our work. Shown are isomer assignments, α-decay energies E_α, relative intensities I_α, reduced α widths δ^2_α, and hindrance factors HF$_\alpha$, energies and multipolarities of coincident γ rays (if known). The γ-ray energy uncertainty is 0.5 keV. The reduced α-decay widths were calculated with the Rasmussen prescription [30] by assuming $\Delta L = 0$ decays. The HF$_\alpha$ values were calculated relative to the strongest α decay within each isomer, for which HF$_\alpha = 1$ was assumed. The panels to the extreme left and right show simplified level sequences and unhindered $\Delta L = 0$ α decays of the neighboring odd-A isotopes ^{193,195}At to the states in the respective daughter nuclides ^{189,191}Bi, modified from Refs. [21,22]. Simplified decay schemes of ^{190}Bi^{m1,m2} are taken from Refs. [8,10]. All spin and parity assignments shown in the figure are tentative and are based on systematics and α-decay and in-beam studies.

summing probability and, thus, to a larger random probability for the ^{194}At$^{m1} \rightarrow {}^{190}$Bi^{m2} correlations. To summarize this discussion, we conclude that the α(7195–7230 keV) group in Figs. 5(h), 5(i), 5(k), and 5(l) seen in prompt and delayed coincidences with the 76-keV γ decay is due to the decay of ^{194}At^{m2} rather than that of ^{194}At^{m1}. The deduced decay data for ^{194}At^{m1} are summarized in Table I and are discussed further below.

E. Production cross sections for ^{194}At and ^{194}Po in the reaction ^{56}Fe + ^{141}Pr → ^{197}At*

The absolute production cross section values of ^{194}At ($3n$ channel) and ^{194}Po (p, $2n$ channel, $E_\alpha = 6842$ keV, not shown in the spectra in this work) were measured at the beam energy of $E(^{56}\text{Fe}) = 255$ MeV in the middle of the target that corresponds to the maxima of the respective excitation functions. The SHIP transmission efficiency was assumed to be 40%.

The total absolute production cross section of $\sigma(^{194}\text{At}) = 1.3(4)$ μb for the sum of both isomers in ^{194}At was deduced from the recoil-α_1 correlation analysis of Fig. 1(a). The relative production of the ^{194}At^{m1} and ^{194}At^{m2} isomers was deduced based on the α_1-α_2 correlation analysis [Figs. 5(a) and 5(g)]. By accounting for the slightly different reported α-branching ratios of the daughter ^{190}Bi^{m1,m2} isomers (see text and Fig. 7), approximately equal production cross sections could be deduced for ^{194}At^{m1} and ^{194}At^{m2} isomers. For ^{194}Po the maximum production cross section was measured as $\sigma(^{194}\text{Po}) = 18(4)$ μb.

IV. DISCUSSION

A. General systematics of the multiplet states in ^{194}At and ^{190}Bi

Spectroscopic studies of the odd-odd Bi and At isotopes are very difficult due to the coupling of the valence protons and neutrons, which results in the multitude of rather closely spaced configurations that are expected in these nuclei; see, e.g., our studies of the odd-odd nuclei $^{184-194}$Bi [8,10,11] and of ^{192}At [12]. Therefore, the first step in our discussion is the inspection of the known decay schemes of the neighboring odd-A ^{191,193,195,197}At isotopes [21,22], which provide direct information on the lowest proton configurations expected in the ^{194}At nucleus. That is why for convenience of the discussion we also show in Fig. 7 the simplified decay schemes of the isotopes ^{193,195}At, modified from those given in Refs. [21,22]. Only the main unhindered $\Delta L = 0$ α decays are shown for these odd-A isotopes in Fig. 7.

We stress here that in the whole discussion below, and also in Fig. 7, the spin and the parity assignments of practically all mentioned states are tentative as no direct measurements were performed so far. These values are mostly based on systematics and on the indirect evidence from the α-decay studies and in-beam work, combined with the tentative spin-parity assignments for the neighboring nuclei ^{191,193,195}At and their daughter Bi isotopes from Refs. [21,22].

It is well known that the ground state of the odd-mass At isotopes with $A \geqslant 197$ has spin-parity $I^\pi = 9/2^-$ and is interpreted as a nearly spherical $\pi 1h^3_{9/2}$ configuration. One of the most important conclusions of studies [21,22] is that the $1/2^+$ state, which is understood as the intruder $\pi 3s^{-1}_{1/2} \otimes \pi 1h^4_{9/2}$ configuration in the spherical shell model, becomes the ground state in ^{191,193,195}At; see Fig. 7. Furthermore, no evidence for the spherical $9/2^-$ state was observed so far in these nuclei. In the deformed mean-field approach this $1/2^+$ state corresponds to the occupation of the $1/2^+[440]$ Nilsson orbital (oblate deformation). (As already discussed in Ref. [28] the labeling follows the standard convention used in the Nilsson model [29] and differs from the one of $1/2^+[400]$ as given in the *Table of Isotopes* [17].) The occurrence of a deformed ground state in the lightest At isotopes is in an agreement with theoretical calculations; see, e.g., Ref. [31], in which a sudden deformation change from $\epsilon_2 \sim 0.06$ to $\epsilon_2 \sim 0.2$ was predicted to happen between ^{199}At and ^{198}At. Furthermore, the oblate-deformed $7/2^-[514]$ Nilsson state, originating from the $\pi 1h_{9/2}$ shell at sphericity and having mixed $\pi 1h_{9/2}/\pi 2f_{7/2}$ character at sufficiently large oblate deformation [21,22], becomes the first excited state situated slightly above the $1/2^+$ ground state in ^{191,193,195}At; see Fig. 7. Finally, in ^{193}At a $13/2^+$ state lying 39(7) keV above the $1/2^+$ state (see Fig. 7) was also observed, which has a spherical $\pi 1i_{13/2}$ configuration.

To summarize, in the nuclei ^{193,195}At, the proton-based $1/2^+$, $7/2^-$, and $13/2^+$ states (where known) are found within $\sim$40 keV of each other and they should be responsible for the lowest states in the odd-odd isotope ^{194}At.

In the respective daughter odd-A isotopes ^{189,191}Bi (see Fig. 7) the nearly spherical $9/2^-$ ground state ($\pi 1h_{9/2}$ configuration) coexists with the low-lying proton-based deformed $7/2^-[514]$, $1/2^+[440]$ and spherical $13/2^+$ states within $\sim$360 keV of each other. Therefore, these configurations are expected to play the dominant role in the odd-odd isotope ^{190}Bi, as discussed in Ref. [8].

The occurrence at low energy of states with markedly different spins and structure leads to isomeric states in both odd-A At and Bi nuclei that results in a quite complex α-decay patterns of the odd-A ^{191,193,195,197}At isotopes [21,22]. The strongest α decays observed in these nuclei are unhindered $\Delta L = 0$ decays feeding the excited states of the same spin, parity, and configuration in the respective daughter nuclides; see Fig. 7. In the context of the following discussion, it is important to note that in all odd-A ^{191,193,195}At isotopes the α decays to the $9/2^-$ ground states of the respective daughters ^{187,189,191}Bi are strongly hindered. This naturally reflects the difference between the parent and the daughter ground-state proton configurations. These observations allow us to provide a qualitative explanation of the observed decay pattern of $^{194}\text{At} \rightarrow {}^{190}$Bi.

In the odd-odd nucleus ^{194}At, due to the proton-neutron coupling, an even more complex situation is expected. From studies of nuclei with lower atomic numbers (e.g., Pt, Hg, Pb, and Po) it is known that by approaching the neutron midshell at $N = 104$, two valence neutrons $\nu 1i_{13/2}$ and $\nu 3p_{3/2}$ play the most important role. Thus, both in the parent odd-odd ^{194}At isotope and in its daughter ^{190}Bi nucleus, one expects a large variety of the closely spaced configurations due to the coupling of the valence protons originating from the $\pi 3s_{1/2}, \pi 2f_{7/2}, \pi 1h_{9/2}$, and $\pi 1i_{13/2}$ orbitals to the valence neutrons from the $\nu 1i_{13/2}$ and $\nu 3p_{3/2}$ orbitals. These configurations are summarized in Table II. As one can see, for the mentioned proton-neutron pairs alone, 34 and 31 closely lying multiplet states are expected in ^{194}At in its daughter ^{190}Bi, respectively.

TABLE II. Main configurations and I^π assignments expected in ^{194}At and its daughter ^{190}Bi. The last column shows the observed states in ^{190}Bi with the tentative I^π assignments which are based on systematics and α-decay data, such as HF_α values and decay characteristics, see discussion in [10].

Configuration	Possible I^π	Observed I^π
^{194}At		
$[\pi 3s^{-1}_{1/2} \times \nu 3p_{3/2}]$	$1^-, 2^-$	
$[\pi 3s^{-1}_{1/2} \times \nu 1i_{13/2}]$	$6^+, 7^+$	
$[\pi 7/2^-[514] \times \nu 3p_{3/2}]$	$2^+ \rightarrow 5^+$	
$[\pi 7/2^-[514] \times \nu 1i_{13/2}]$	$3^- \rightarrow 10^-$	
$[\pi 1i_{13/2} \times \nu 3p_{3/2}]$	$5^- \rightarrow 8^-$	
$[\pi 1i_{13/2} \times \nu 1i_{13/2}]$	$0^+ \rightarrow 13^+$	
^{190}Bi		
$[\pi 1h_{9/2} \times \nu 3p_{3/2}]$	$3^+ \rightarrow 6^+$	(3^+)
$[\pi 1h_{9/2} \times \nu 1i_{13/2}]$	$2^- \rightarrow 11^-$	(10^-)
$[\pi 1h_{9/2} \times \nu 1h_{9/2}]$	$0^+ \rightarrow 9^+$	
$[\pi 7/2^-[514] \times \nu 3p_{3/2}]$	$2^+ \rightarrow 5^+$	
$[\pi 7/2^-[514] \times \nu 1i_{13/2}]$	$3^- \rightarrow 10^-$	
$[\pi 3s^{-1}_{1/2} \times \nu 3p_{3/2}]$	$1^-, 2^-$	
$[\pi 3s^{-1}_{1/2} \times \nu 1i_{13/2}]$	$6^+, 7^+$	

Based on the systematics of the neighboring odd-A nuclei, the lowest observed α-decaying states in ^{190}Bi should be due to the $\pi 1h_{9/2}$ configuration, coupled to the $\nu 1i_{13/2}$ and $\nu 3p_{3/2}$ neutrons. These inferences were indirectly confirmed by α-decay studies [8,10], which identified the (10^-) and (3^+) isomeric states in ^{190}Bi; see Table II and Fig. 7.

B. ^{194}At^{m2}

In ^{194}At, based on the systematics of the neighboring odd-A isotopes, one does not expect the low-lying $\pi 1h_{9/2}$-based states. Thus the lowest α-decaying states observed in this nucleus are most probably due to the oblate-deformed $1/2^+[440]$ or $7/2^-[514]$ proton configurations, which are the lowest in the neighboring odd-A nuclei. This readily explains the very large hindrance factor for the highest-energy 7310-keV decay of ^{194}At^{m2}, see Fig. 7 and Table I. In this respect, the decay schemes of ^{194}At^{m2} and of ^{191,192,193,195}At nuclei are similar, with the highest energy α decays being strongly hindered in all of them.

However, the strongest 7190-keV decay of ^{194}At^{m2} feeds an excited state at 121(15) keV in its daughter. This pattern is similar to the decay of the neighboring ^{193,195}At nuclei, in which there exist unhindered α decays to the low-lying $1/2^+$ and/or $7/2^-$ excited states in the excitation energy region of $E^* = 100$–242 keV in ^{189,191}Bi; see Fig. 7. The feeding of the possible $13/2^+$-proton based state in ^{190}Bi is most probably excluded due to the much higher excitation energy of $E^*(13/2^+) = 358$ keV in ^{189}Bi (Fig. 7). Actually, the 7190-keV decay of ^{194}At^{m2} is slightly hindered [by a factor of 4.8(6)] relative to the $\Delta L = 0$ unhindered decays in ^{193,195}At. This HF_α value was calculated relative to the average value of $\delta_\alpha^2 = 58(7)$ keV for unhindered $7/2^- \rightarrow 7/2^-\alpha$ decays in ^{191,193,195}At [21,22]. We notice that the 7190-keV decay is also hindered by a similar factor of $\sim$4.8(9) relative to the unhindered $(3^+ \rightarrow 3^+)$ 6431-keV decay of ^{190}Bi^{m2}; see Fig. 7 (right panel).

Due to a relatively moderate hindrance factor for the 7190-keV decay we suggest that, most probably, both the respective parent and daughter states connected by this decay are based on the same oblate-deformed proton configuration (either the $1/2^+[440]$ or $7/2^-[514]$) coupled to same neutron configuration (either the $\nu 1i_{13/2}$ or $\nu 3p_{3/2}$). We also notice that, according to calculations [31], an oblate deformation of $\epsilon_2 \sim 0.22$ should be expected in ^{194}At. However, based on the observed decay pattern of ^{194}At^{m2} and by considering that in the neighboring odd-A ^{191,193,195}At nuclei the energy separation between the $1/2^+$ and $7/2^-[514]$ states is very low (see Fig. 7), we cannot draw an unambiguous conclusion on the exact configuration of the 253(10) ms isomer in ^{194}At.

Other fine structure α decays of ^{194}At^{m2} observed in our study are more strongly hindered than the 7190-keV decay. Therefore, they proceed either to the different multiplet states in ^{190}Bi^{m2} or they proceed with a change of the proton and/or neutron configuration. As discussed in Sec. III, the low-energy strongly converted prompt γ-ray transitions between the multiplet states complicate enormously the data analysis and the interpretation of the results, which is why we prefer to limit our discussion at the present level.

C. ^{194}At^{m1}

The decay pattern of ^{194}At^{m1} differs somewhat from that of ^{194}At^{m2}, as in this case the strongest 7178-keV decay feeds directly the presumed long-lived α-decaying isomeric 10^- state in ^{190}Bi rather than one of the excited states. The 7178-keV decay is also slightly hindered $[\mathrm{HF}_\alpha = 5.8(9)]$ relative to the unhindered decays of the odd-A neighbors (see discussion above). Furthermore, it is also slightly hindered $[\mathrm{HF}_\alpha = 3.3(9)]$ relative to the unhindered $(10^- \rightarrow 10^-)$ 6456-keV decay of ^{190}Bi^{m1}; see Fig. 7 (left panel). Such a moderate hindrance factor suggests that the parent configuration in ^{194}At^{m1} should be quite similar but still differs somewhat from that of the spherical $[\pi 1h_{9/2} \times \nu 1i_{13/2}]_{10^-}$ daughter state in ^{190}Bi^{m1}. In our opinion, such a configuration could be still based on the $7/2^-[514]$ Nilsson proton orbital, originating from $1h_{9/2}$ at sphericity and having a mixed $1h_{9/2}/2f_{7/2}$ character at a sufficiently large oblate deformation. In such a case, one of the lowest-lying 9^- or 10^- states from the $[\pi 7/2^-[514] \times \nu 1i_{13/2}]_{3^- - 10^-}$ multiplet should represent the state in ^{194}At^{m1} decaying by the 7178-keV decay.

Interestingly, the situation in ^{194}At^{m1} is clearly different to the case of ^{192}At^{m1}, in which the highest-energy 7385-keV decay is hindered by a factor of 20(4); see Fig. 7 of Ref. [12]. In the case of ^{192}At^{m1}, however, the parent state is believed to be based on a well-defined oblate-deformed $[\pi 7/2^-[514] \times \nu 1i_{13/2}]$ configuration; see the discussion in Ref. [12], the decay of which to the spherical $[\pi 1h_{9/2} \times \nu 1i_{13/2}]_{10^-}$ daughter state in ^{188}Bi^{m1} is hindered.

Therefore, if ^{194}At^{m1} is indeed based on the $7/2^-[514]$ Nilsson proton orbital, then to explain smaller hindrance factor for the 7178-keV decay we have to assume that both the degree of mixing with the $\pi 2f_{7/2}$ orbital and the onset of oblate deformation are somewhat smaller in ^{194}At^{m1} in comparison with ^{192}At^{m1}.

Unfortunately, based on available information, no unambiguous discussion of the possible spin-parity assignments can be given for the fine-structure α decays at 6908, 7085, and 7135 keV.

V. CONCLUSIONS

The detailed α-decay study of ^{194}At isotope was performed in the complete fusion reaction of ^{56}Fe ions with the ^{141}Pr target. The high statistics collected in our experiment, along with the efficient and versatile detection system, allowed us to identify two α-decaying isomeric states in this nucleus. Complex decay schemes for both isomers were deduced and discussed in the article. Due to this complexity and the large number of possible coexisting structures both in the parent ^{194}At and in the daughter ^{194}Bi nuclides, no unambiguous configuration assignments are possible. Nevertheless, a comparison with the neighboring isotopes ^{191,192,193,195}At suggests that the oblate-deformed configurations based on the $1/2^+[440]$ and/or $7/2^-[514]$ orbitals become the lowest in

^{194}At. Therefore, these data provide extended evidence for the deformed nature of the lightest odd-odd At isotopes. However, the smaller hindrance factor values in ^{194}At in comparison with ^{192}At might indicate that the oblate deformation is somewhat smaller in ^{194}At. Thus ^{194}At should be considered as a "transitional" nucleus between the spherical heavier At isotopes and oblate-deformed lighter At isotopes.

Future experiments aimed to studies of these nuclei must envisage an efficient detection system in which both the low-energy electrons and low-energy x rays could be measured. A possible way how to study these nuclei under cleaner conditions could involve the use of a mass separator, such as ISOLDE at CERN, along with the isomer separation by using the laser ionization technique.

ACKNOWLEDGMENTS

A.N.A. and J.J.R. were partially supported by the NSERC of Canada. We thank the UNILAC staff for providing the stable and high-intensity ^{56}Fe beams. This work was supported by FWO-Vlaanderen (Belgium), GOA/2004/03 (BOF-K.U.Leuven), and the "Interuniversity Attraction Poles Programme—Belgian State Belgian Science Policy" (BriX network P6/23), by the European Commission within the Sixth Framework Programme through I3-EURONS (Contract RII3-CT-2004-506065), and by United Kingdom Science and Technology Facilities Council. S.A. and S.S. were supported by the Slovak Research and Development Agency under contract no. APVV-20-006205.

[1] A. N. Andreyev *et al.* (in preparation, 2009).
[2] H. L. Hall and D. C. Hoffman, Annu. Rev. Nucl. Part. Sci. **42**, 147 (1992).
[3] D. A. Shaughnessy *et al.*, Phys. Rev. C **65**, 024612 (2002).
[4] A. N. Andreyev *et al.*, Phys. Lett. **B312**, 49 (1993).
[5] J. Van Maldeghem and K. Heyde, Fizika **22**, 233 (1990).
[6] A. J. Kreiner, C. Baktash, G. GarciaBermudez, and M. A. J. Mariscotti, Phys. Rev. Lett. **47**, 1709 (1981).
[7] M. Huyse *et al.*, Phys. Lett. **B201**, 293 (1988).
[8] P. Van Duppen *et al.*, Nucl. Phys. **A529**, 268 (1991).
[9] P. Van Duppen and M. Huyse, Hyperfine Interact. **132**, 141 (2001).
[10] A. N. Andreyev *et al.*, Eur. Phys. J. A **18**, 39 (2003).
[11] A. N. Andreyev *et al.*, Eur. Phys. J. A **18**, 55 (2003).
[12] A. N. Andreyev *et al.*, Phys. Rev. C **73**, 024317 (2006).
[13] S. Yashita, thesis, LBL-15562 (1984), unpublished.
[14] M. Leino *et al.*, Acta Phys. Pol. B **26**, 309 (1995).
[15] G. Münzenberg *et al.*, Nucl. Instrum. Methods **161**, 65 (1979).
[16] S. Hofmann *et al.*, Z. Phys. A **291**, 53 (1979); S. Hofmann and G. Münzenberg, Rev. Mod. Phys. **72**, 733 (2000).
[17] R. B. Firestone, *Table of Isotopes*, 8th ed. (John Wiley & Sons, Inc., New York, 1996).
[18] K. Van de Vel *et al.*, Phys. Rev. C **68**, 054311 (2003).
[19] J. Wauters, P. Dendooven, M. Huyse, G. Reusen, P. VanDuppen, P. Lievens, and The ISOLDE Collaboration, Phys. Rev. C **47**, 1447 (1993).
[20] S. Saro *et al.*, Nucl. Instrum. Methods A **381**, 520 (1996).
[21] H. Kettunen *et al.*, Eur. Phys. J. A **16**, 457 (2003).
[22] H. Kettunen *et al.*, Eur. Phys. J. A **17**, 537 (2003).
[23] C. Webber *et al.*, Nucl. Phys. **A803**, 1 (2008).
[24] T. Kibédi *et al.*, Nucl. Instrum. Methods A **589**, 202 (2008); conversion coefficients calculator BrIcc v2.2a, http://wwwrsphysse.anu.edu.au/nuclear/bricc/.
[25] F. P. Heßberger *et al.*, Nucl. Instrum. Methods A **274**, 522 (1989).
[26] A. N. Andreyev *et al.*, Nucl. Instrum. Methods A **533**, 409 (2004).
[27] A. N. Andreyev *et al.*, Eur. Phys. J. A **10**, 129 (2001).
[28] A. N. Andreyev *et al.*, Phys. Rev. C **69**, 054308 (2004).
[29] P. Ring and P. Schuck, *The Nuclear Many-Body Problem* (Springer-Verlag, New York, 1980), p. 75.
[30] J. O. Rasmussen, Phys. Rev. **113**, 1593 (1959).
[31] P. Möller *et al.*, At. Data Nucl. Data Tables **59**, 185 (1995).